In situ TEM investigations of dendritic growth of Au particles on HOPG

R. Anton and I. Schneidereit
Institut für Angewandte Physik und Zentrum für Mikrostrukturforschung, Universität Hamburg, Jungiusstraße 11, D-20355 Hamburg, Germany

(Received 8 May 1998; revised manuscript received 7 July 1998)

Gold was vapor deposited onto thin substrates of highly oriented pyrolytic graphite at room temperature inside a transmission electron microscope, which was modified for *in situ* experimentation. The kinetics of nucleation and dendritic growth of particles was recorded in real time. Two growth modes of particles were observed on different parts of the substrate. Small particles with high nucleation density populated defective substrate areas, where condensation was complete, as was verified by quantitative analysis of x-ray fluorescence, while on virtually undisturbed areas, the nucleation density was much lower, condensation initially incomplete, and particles grew dendritic. The lateral growth speeds of the latter were found to be strongly correlated to the sizes of the respective capture areas. This is attributed to similar heights of the particles, starting at about 1 nm soon after nucleation. The growth kinetics of individual aggregates were compared with a diffusion model, which allowed us to estimate the adatom mean diffusion length before desorption to about 400 nm. Relying on a value for the surface lifetime of a gold adatom of less than 10 ms at room temperature, as reported in the literature, this results in an upper limit for the diffusion barrier of 0.24 eV on graphite. [S0163-1829(98)04643-8]

I. INTRODUCTION

Dendritic growth of crystals is a rather common phenomenon in nature, but it is more an exception in vapor deposition experiments. At least for metals on substrates such as dielectrics or ionic crystals, three-dimensional growth of particles is usually thermodynamically favored, especially at elevated temperatures. However, under certain circumstances, kinetic limitations may prevent three-dimensional growth, for example when the adatom diffusivity is high on the substrate, but lower on aggregates of its own kind. Another reason may be the existence of a diffusion barrier at particle edges or facets. This seems to be the case for gold on single-crystalline graphite at temperatures below about 100 °C. As this system can be handled relatively easily experimentally, it has attracted much attention in the past with the aim to understand this peculiar type of adatom aggregation. In the ''classical'' work of Darby and Wayman, it was already established that dendritic growth requires clean substrate surfaces, otherwise the metal nucleates finely dispersed.[1] A clean substrate can be obtained by cleaving the graphite in vacuum prior to the deposition of gold. Air-cleaved substrates must be extensively heated in vacuum in order to obtain at least some virtually clean areas. Métois has investigated the influence of the vacuum conditions, especially of the type of vacuum pump, on the cleanliness of cleavage surfaces, as judged from the degree of perfection of dendritic growth.[2] As a result, charged particles, delivered from an ion getter pump, may produce defects on the graphite surface plane, causing the nucleation and growth of many small, compact particles.

Darby and Wayman presented a qualitative model of dendritic growth, which is based on anisotropic diffusion sinks around protrusions of a growing particle.[3] These authors correlate the occurrence of two typical growth directions of dendrites, $[110]_{Au}\|[1\bar{0}10]_{graphite}$ and $[112]_{Au}\|[2\bar{1}\bar{1}0]_{graphite}$, with the adatom flux. When this is high, aggregation is more two-dimensional, because three-dimensional rearrangement is hindered, and islands are bounded by the slowest growing edges, leading to growth in the [110] direction. In contrast, at lower flux, more three-dimensional growth occurs, with the slowest growing planes as boundaries, and dendrites are directed along the [112] direction. A change of the flux from high to low, which may take place, for example, when competitive capture by neighboring particles becomes significant, would cause a corresponding change of the growth direction of the dendrites. Experiments seem to confirm this view.

Dendritic growth has often been described with ''diffusion limited aggregation'' (DLA), as modeled, for example, by Witten and Sander.[4] This means basically that an adatom performs a random walk on the substrate, but will be captured by a growing aggregate upon any encounter. With little or no diffusion along the edge of the aggregate, this leads to extremely ramified structures, with rather low ''fractal dimension'' ($\sim$1.7), and which do not resemble very well those found experimentally for gold on graphite. Wynblatt *et al.* have performed similar simulations, but allowed reduced sticking probabilities of adatoms at the circumference of a particle, depending on the nearest-neighbor configuration.[5] This approach in effect simulates atom diffusion along the circumference of a particle, leading to more compact aggregation. Significantly higher fractal dimensions ($\sim$1.9) could be obtained with this method, being close to experimental examples. Both approaches certainly deliver important contributions to the understanding of dendritic growth. However, quantitative data on the kinetics of adatom diffusion and capture are still lacking.

We have performed deposition experiments *in situ* in an electron microscope, and analyzed the growth kinetics of individual aggregates by measuring the rates of adatom capture directly, locally resolved, and in real time (which means television rate). The aim was to obtain further insight into the

adatom processes of diffusion and capture, which govern dendritic growth. In particular, the ''*in situ* approach'' allows us to assess the influence of competitive capture by neighboring aggregates quantitatively, such that particle growth rates are directly correlated with the sizes of the surrounding capture areas. Moreover, evidence was found that particles generally grow with similar heights from the beginning, and mainly laterally, while the contribution of direct impingement becomes significant only at later stages. This allows us to estimate the adatom diffusivity on the substrates on the basis of a model of adatom diffusion and capture, which takes into account an initial condensation coefficient of much less than unity on the bare substrate, even at room temperature.

II. EXPERIMENTAL PROCEDURES

Vapor depositions of gold on graphite substrates were performed in a transmission electron microscope (Philips EM400), which had been modified for *in situ* experimentation. The metal was evaporated from a Knudsen-like cell located in a chamber attached to the goniometer stage of the microscope, which was differentially pumped by a turbomolecular pump with magnetic bearings. The vapor beam flux was monitored with a quadrupole mass spectrometer. After mild baking of the evaporation chamber, and eventually also of the microscope column, the base pressure in the specimen region was in the mid 10^{-9}-mbar range, with the cold finger at liquid nitrogen temperature. During deposition experiments, the pressure rose to $(1-2)\times10^{-8}$ mbar. Virtually no hydrocarbons could be detected with the mass spectrometer. Particle nucleation and growth was imaged via a closed circuit television (CCTV) chain, and was recorded on video tape [super video home system (S-VHS) (VHS is a standard video format)]. By using an electronic image intensifier, and not too high magnifications, the electron beam density on the specimen could be kept below 1 A/cm^2, which is about one order of magnitude lower than needed for normal imaging. More details of the apparatus have been described in earlier papers.[6]

Thin, electron transparent substrates of highly oriented, pyrolytic graphite (HOPG) were prepared in the usual way: A prethinned graphite flake was cemented onto a special transmission electron microscope (TEM) specimen grid of molybdenum. Final thinning was done by pulling off several layers with adhesive tape bonded to the surface, until the specimen became transparent for light. In most cases, this indicated the existence of some areas being sufficiently thin for imaging in the TEM. Then, the sample was immediately transferred into the microscope, where it was heated up to 600 °C for several hours. The cleanliness of the surface was judged from the appearance of the gold aggregates in the subsequent depositions at room temperature, according to results of other authors already cited.[1–3] The deposition rate was kept constant at 2×10^{12} atoms/cm^2 s. Calibration was done by depositions on amorphous carbon, for which complete condensation at room temperature has been established, using quantitative energy-dispersive analysis of x-ray fluorescence (EDX).[6] Flat islands with dendritic structures were obtained on virtually clean areas, while small particles with compact shapes were found to nucleate with high number densities on apparently defective areas, which were found to be inhomogeneously distributed on the samples. The nature of the defects could not be determined. At least, we tend to exclude contamination, either caused by residual gases or by ions from the ion getter pump, as this would be expected to produce a more homogeneous distribution of decoration. It appears that nucleation is generally much more sensitive to defects or contamination on the substrate than any analytic or microscopic tool. Possibly, we deal with intrinsic defects within the HOPG layers, which may require much higher temperatures for healing than applied in our experiments. The chances to find undisturbed areas could be somewhat improved by preheating the substrate under an elevated partial pressure of oxygen of 7×10^{-6} mbar.

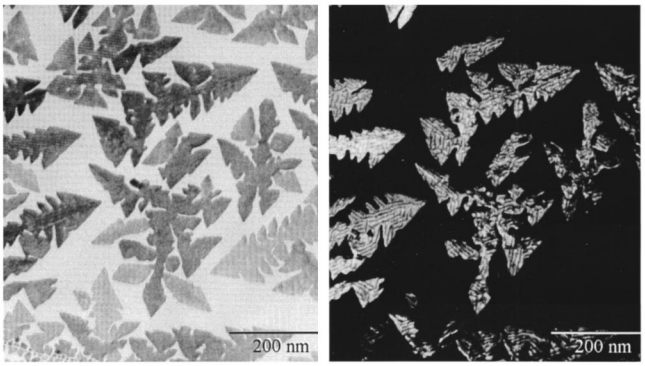

FIG. 1. Bright field (left) and dark field image (right) of dendritic particles on HOPG. The rather uniform contrast in the former and the Moiré stripes in the latter indicate flat surfaces of the dendrites. Slight variations of Bragg contrast in different dendrites and the absence of some dendrites in the dark field image originate from different epitaxial orientations.

When imaging nucleation and growth of particles during condensation, one has to be concerned about the influence of the electron beam. In fact, a slight effect may be indicated, when comparing Figs. 1 and 2 below. The former image was taken on film after the end of deposition, without exposing the sample to the electron beam during deposition, while Fig. 2 shows video images taken during growth. The more pronounced faceting in the former case and the more ramified structures in the latter are evident. We believe that this effect is due to a higher net mobility of the gold adatoms when no electrons are present. However, we did not find any clues as to whether electron bombardment produces defects or contamination. At least, a possible local rise of the temperature would probably cause the opposite effect, which, however, could be overcompensated by the pinning effect of ''defects.'' Nevertheless, in total, the influence of the electron beam does not seem to be dramatic. In fact, the morphologies of the islands compare well with those found, for example, by Darby *et al.*[1] on vacuum cleaved substrates, with no electron irradiation during condensation. We deem this as confirmation that our approach of *ex situ* cleaving, *in situ* heating under oxygen, and low dose imaging yields sufficiently clean areas and virtually undisturbed growth.

After the end of deposition, the amount of gold was measured by quantitative EDX in another TEM, either averaged over larger areas or locally, in order to determine the overall condensation coefficient and the masses of individual particles, respectively. This allowed us to estimate the thickness

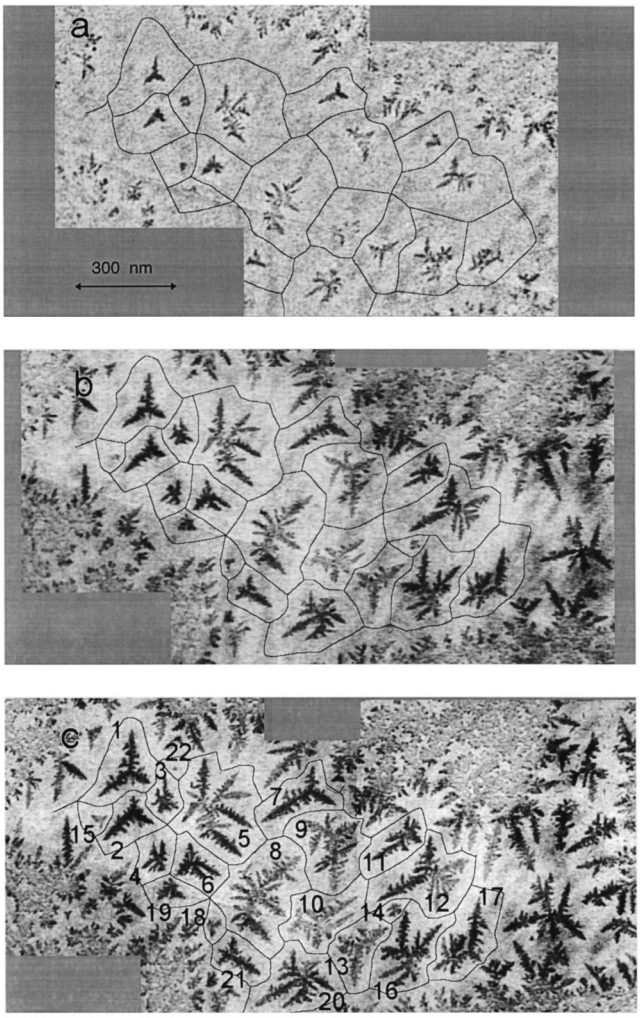

FIG. 2. Video images taken during growth of gold particles on HOPG at room temperature. Dendritic shapes develop on virtually undisturbed substrate areas, while high nucleation densities in surrounding areas are attributed to decoration of defects. The solid lines indicate the estimated distribution of capture areas. Deposition times were 765 s (a), 1750 s (b), and 3240 s (c).

of the aggregates. Substrate coverage, projected areas of particles and of individual dendrites, and the sizes of the capture zones were measured by means of quantitative image analysis. This usually required considerable image processing and contrast enhancement, which was facilitated by averaging over several consecutive frames in the video sequences.

III. RESULTS

A. General observations

In the first part of our experiments, we compared typical details of dendritic growth of gold on our HOPG substrates with those reported by other authors for growth on natural graphite. Epitaxial orientation with $(111)_{Au}\|(0001)_{graphite}$ and $[112]_{Au}\|[2\bar{1}\bar{1}0]_{graphite}$ was verified from diffraction analysis, as was expected for our low rate conditions.[1] The latter is the growth direction of the primary dendrites. Also, dark field imaging with $\frac{1}{3}(422)$ reflections of gold revealed double-positioning of crystallites, as was already described by Darby *et al.*[1] Further, stripes in dark field images, being parallel to the growth directions of primary as well as of secondary branches, are interpreted as a sort of Moiré pattern, being caused by a (23×1) superstructure on the (111) surface of the gold. This implies a contraction of the surface layer in the [110] directions, perpendicular to [112].[7] Both, double-positioning and Moirés are demonstrated in Fig. 1. The reason why we emphasize these observations is because they suggest that the gold islands exhibit virtually planar surfaces. Moreover, the more or less uniform contrast, which is observed for most aggregates when not in Bragg position, indicates about equal thicknesses. Average thickness values were calculated from quantitative measurements of the substrate coverage and of the deposited mass of gold by EDX, yielding values of the order of 1 to 2 nm. Possible reasons for the development of flat islands will be discussed below.

Interesting observations were made regarding the mobility of particles. While dendritic aggregates were never seen to drift across the substrate, small particles, which had not yet developed dendrites, sometimes performed sudden jumps (see, for example, particle no. 14 in Figs. 2 or 6 below), or flipped over their edges landing upside down. Such movements mostly occurred from one TV frame to the next, e.g., within <20 ms. Often, particles jumped forth and back several times, until growing too large. Sometimes, consecutive jumps resulted in directional ''slow motion.'' The origin of the driving force is not quite clear, but is believed to be due to charging by the electron beam.

Further insight into the kinetics of nucleation and growth of the particles was obtained from sequential imaging during condensation. This will be discussed in Sec. III C.

B. Condensation coefficients

EDX measurements of the condensed mass of gold on graphite were performed following depositions for various times. These data were ratioed to the vapor beam dose being offered to the substrate, so as to obtain the integrated condensation coefficient. As a result, condensation was found to be complete, from the start of deposition, on the disturbed areas, where particles grow finely dispersed with more or less rounded, compact shapes. In contrast, on undisturbed areas, where particles grow dendritic, condensation was incomplete at the early stages. After 500 s of deposition, at a projected coverage of about 5%, the integrated condensation coefficient was of the order of $30\pm20\%$, and estimated to be much lower initially, but rapidly approached unity at later stages, although the projected coverage did not exceed about 40% after the end of deposition. This is in qualitative agreement with results from Arthur and Cho, obtained from atomic scattering experiments.[8] These authors reported a condensation coefficient of below 0.05 for the first few seconds of deposition, also at room temperature, and at a slightly greater vapor beam flux, but increasing within 500 s to unity. Although the morphology of the deposits was not investigated in that work, our TEM observations suggest that the increase of the condensation coefficient with deposition time (hence coverage) is primarily due to an increasing capture probability for adatoms diffusing on the substrate, rather than due to direct impingement from the vapor beam. This will be discussed in more detail below.

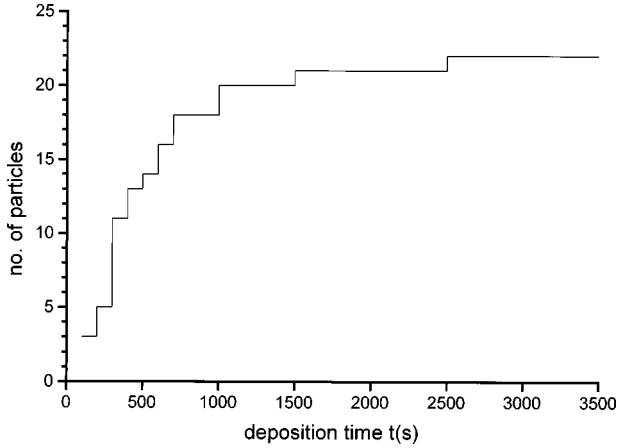

FIG. 3. The evolution with deposition time of the population of dendritic particles within the capture areas marked in Fig. 2. The saturation value corresponds to a number density of about $3\times10^9/\mathrm{cm}^2$. The individual times of nucleation were extrapolated from the dependence of particle size vs time (see, for example, Fig. 7 below).

C. Nucleation and growth

Figure 2 shows a representative series of video images of the nucleation and growth of a larger number of gold particles on HOPG at room temperature. On a supposedly ''clean'' area (see Sec. II) with total size of about 3 $\mu\mathrm{m}^2$, dendritic particles are growing with initial distances between the first appearing nuclei of several hundred nm. This area is surrounded by a selvedge of particles, which also produce dendrites, when growing inwards, whereas particles outside of the selvedge nucleate finely dispersed, indicating the existence of some kind of defects on that part of the substrate surface, as discussed above. Within the undisturbed area, the capture zones of individual aggregates are indicated by contour lines, which were drawn by hand by estimating the points of equal probability of an adatom being captured by one or another neighboring aggregate, assuming isotropic diffusion. Most dendrites were found to grow in epitaxial orientation, as was already mentioned above. Deviations are not uncommon, and probably originate from crystallographic defects (see particles no. 5 and 8). In any case, the growth direction seems to be mainly determined by the crystallography of the gold, but not so much by that of the graphite.

The kinetics of nucleation is illustrated in Fig. 3, where the number of dendritic aggregates within the field in Fig. 2, which is marked by capture areas, is plotted versus deposition time. After a rapid initial increase of the number of particles, saturation is approached at a value that corresponds to a number density of about $3\times10^9/\mathrm{cm}^2$. On other areas, which had not been irradiated with electrons during deposition, densities were in the upper $10^8/\mathrm{cm}^2$ range. These values are higher than those from other authors, obtained on samples of natural graphite. Métois *et al.* reported a value of $3\times10^8/\mathrm{cm}^2$ for vacuum cleaved graphite and at a similar equivalent mean thickness of gold,[2] while data from Darby *et al.* are as low as $6\times10^7/\mathrm{cm}^2$, although at a lower equivalent mean thickness.[1] These differences may indicate an influence of the electron beam, but we tend to believe that the defect density is intrinsically higher on our HOPG substrates. On the obviously defective areas, where particles nucleate finely dispersed, saturation densities were generally higher by about two orders of magnitude, but still about two orders lower than on amorphous carbon, under similar conditions.[9]

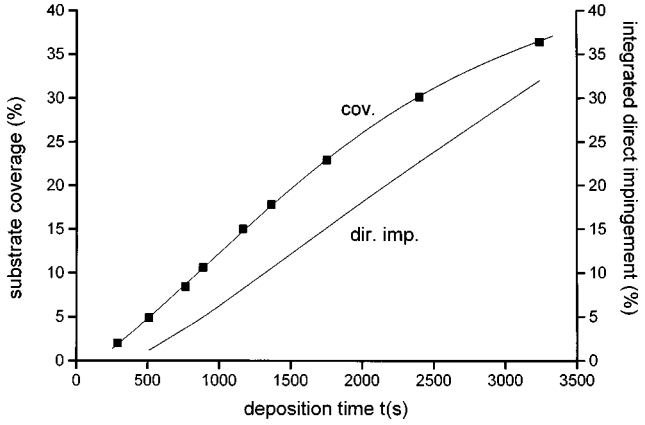

FIG. 4. Increase with deposition time of the substrate coverage of dendritic particles in Fig. 2 (data symbols, left-hand axis). The s-shaped solid line is a regression curve. Also plotted is the fractional, integrated contribution of direct impingement to the volume of the particles (right-hand axis), as calculated from the vapor beam flux and the increase of coverage.

In Fig. 4, the increase of the substrate coverage is plotted versus deposition time. One can see that the growth rate initially increases, stays about constant up to about 20% coverage, but slows down significantly thereafter. This peculiar behavior was also found for individual particles and will be discussed in more detail below. From the substrate coverage and the condensed mass, as discussed in Sec. III A, the average height of the dendritic aggregates was calculated to about 1 nm at the early stages, increasing to about 1.5–2 nm at the end of deposition. These estimates correspond to scanning tunneling microscopy (STM) results by Nishitani *et al.*, who measured particle heights of about 1.7 nm.[10]

D. Competitive capture

The preferred lateral growth of dendritic aggregates offers the unique possibility to study the influence of competitive

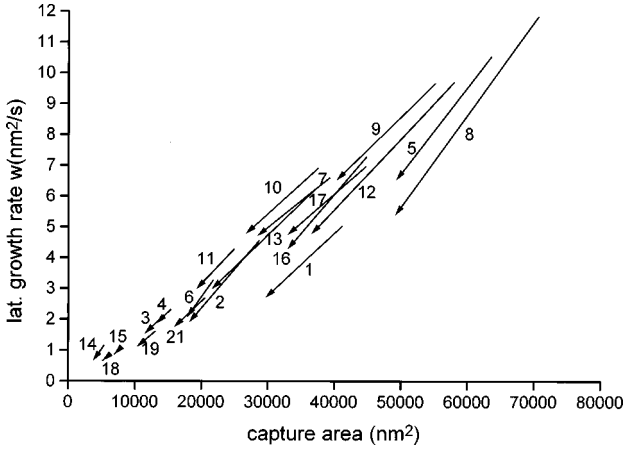

FIG. 5. Variation of the lateral growth speed of 20 of the numbered particles in Fig. 2 with their individual capture areas. Arrows indicate the decrease of the growth speed from an initial maximum value (see Fig. 8) to the respective values at the end of deposition, at $t=3240$ s.

capture in much more detail than is possible in the case of 3D growth. In Fig. 5, the growth rates of 20 particles imaged in Fig. 2 are plotted versus their individual capture areas. For each particle, the decrease of the growth speed, from the initial maximum value (see below), with decreasing size of the respective capture area is indicated by an arrow, pointing in the direction of increasing deposition time. Interestingly, the growth speeds of most particles follow about the same curve, with relatively little scatter. This means that the heights of the particles cannot be very different, as was already suggested by their similar contrast.

A rough estimate of the vertical growth rate of the particles was made from the measured increase with time of the projected particle areas, and from the integrated contribution of direct impingement (see Fig. 4), calculated with a deposition rate of 2×10^{12} atoms/cm^2 s. Assuming that only direct impingement contributes to vertical growth, this would result in an increase in height by not more than 1 nm from the instant of nucleation up to the end of deposition. Taking into account an initial height of about 1 nm, as was discussed above, the contribution of direct impingement to the volume of the particle would be less than 10% within the first 1200 s of deposition, and about 33% at the end of deposition. Then, the average height would not exceed about 2 nm. This estimate agrees surprisingly well with calculations based on measurements of the substrate coverage, and of the condensed mass, as mentioned in Sec. III C. Thicknesses in the range of only a few nm appear reasonable, as judged from the contrast in the TEM images. Only a few particles were found to grow significantly slower than the average, in particular nos. 1, 8, and perhaps 5. Possibly, particle no. 1 grows intrinsically higher, which is indicated by its greater than normal contrast. Deviations of the growth rates from proportionality can be explained by variations of the particle heights of not more than 50%. The especially faster than average decay of the growth rates of particles no. 8 and 5 may be caused by some local recrystallization. This could be correlated with their ramified shapes. Another source for scatter of the data may be the determination of the sizes of the capture areas. The error of the measurement was estimated to the order of 5% from the variations of data taken at different deposition times.

More details of the growth kinetics as well as of the role of competitive capture are revealed by local analysis of images taken at higher magnification. Figure 6 shows an enlarged view of the group of particles no. 11, 12, and 14, together with parts of neighboring aggregates (refer to Fig. 2). It is a superposition of contours, drawn at about equal amounts of elapsed times. The corresponding increase of the projected areas of the aggregates is color coded so as to visualize the local growth kinetics, as well as the simultaneous development of substrate coverage in the neighborhood. Particle no. 12 nucleated at about 100 s after opening the shutter, particle no. 11 at about 200 s, while the nucleus of particle no. 14 appeared only after 1000 s. As stated above, particle shapes are initially rather compact, and growth of primary dendrites starts with high speed at protrusions in the designated crystallographic directions. During further growth, the influence of competitive capture by neighboring aggregates is apparent when comparing the evolution with time of individual dendrites, for example nos. *A* and *B* of particle no. 12. These images clearly support that the local lateral growth speed of the dendrites is mainly determined by the supply of diffusing adatoms from the net capture areas. The development of long narrow channels and even holes should be noted, which are filled only very slowly. This may be caused by the existence of an energetic barrier for adatoms diffusing on the particle mesas for descending over the edges, and will be discussed in more detail below. The increase with deposition time of the projected areas of particles no. 11, 12, and 14 is plotted in Fig. 7. The s-shaped fitting curve, which is most pronounced for particle no. 12, should be noted. The growth rate increases until the dendrites are fully developed, but decreases later with increasing coverage. As will be discussed in the following, this

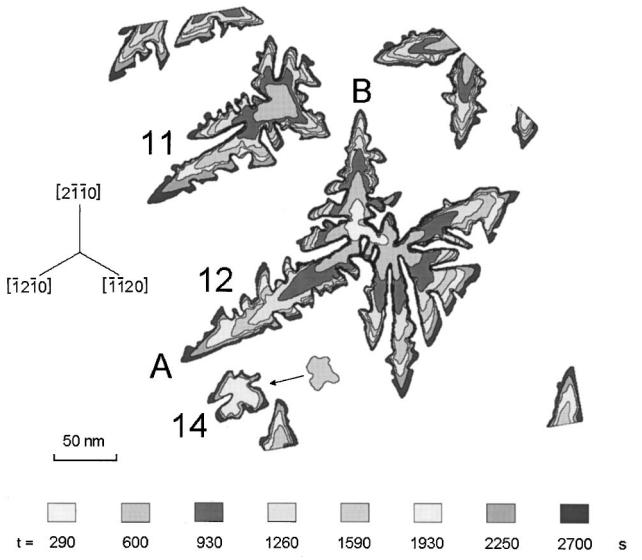

FIG. 6. Superposition of contour plots of the area with particles 11, 12, and 14 (refer to Fig. 2), taken at approximately equal time steps, as indicated by different gray values. Capital letters denote dendrites growing in principal directions of the graphite lattice, as indicated. Growth speeds of individual dendrites are high in directions of free space (*A*, for example), but slow down significantly when approaching neighboring aggregates (*B*). Particle no. 14 performed a sudden jump at about $t=1300$ s.

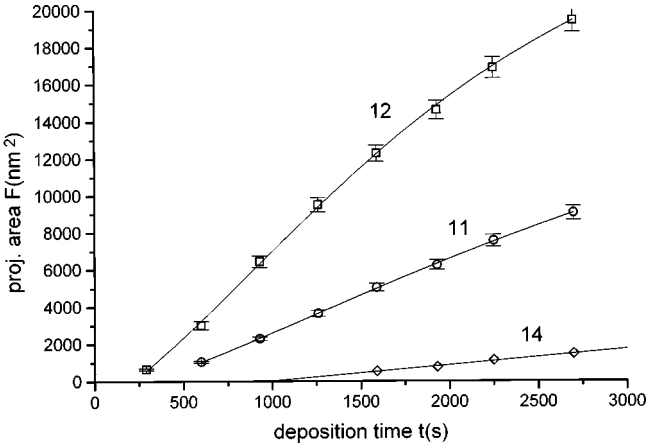

FIG. 7. Plot of the projected areas F vs deposition time t for particles 11, 12, and 14. Curves are polynomial fits to the data points. Note, for particle no. 12, the s-shaped fitting curve.

can be explained by the superposition of the increase of the capture probability with particle size and the effect of decreasing capture areas.

IV. DISCUSSION

Major parameters influencing nucleation and particle growth kinetics are the energies of surface diffusion and adsorption on the substrate as well as on the particles. In addition, the number and sort of defects and the thermodynamical tendency to form equilibrium shapes play a role. Much experimental and theoretical work has been done to assess this quantitatively. Comprehensive reviews are given, for example, by Venables *et al.*[13,14] However, for the system Au/graphite, quantitative data are rather limited.

Arthur and Cho have investigated the condensation coefficient of gold on the surface of graphite by atomic scattering experiments and found initially incomplete condensation already at room temperature.[8] For the first few seconds of deposition, an instantaneous condensation coefficient α of less than 0.05 is reported, at a slightly greater deposition flux than in our experiments. Their data suggest an increase to unity within about 500 s. Our EDX measurements also suggest an upper limit in this range, although the approach to unity is much slower in our experiments. Incomplete condensation means that the adatom lifetime $\tau = \tau_0 \exp(E_a/kT)$ on the substrate surface is determined by the adsorption energy E_a, rather than by capture by other aggregates or defects, as long as the respective distances are greater than the mean diffusion path $\lambda = (D\tau)^{0.5}$ before desorption, where D is the diffusion coefficient. In fact, Arthur and Cho reported lifetimes of below 10 ms at 300 K for Au and Cu atoms on graphite.[8] This would correspond to an upper limit of E_a of 0.64 eV, when assuming a preexponential factor of 10^{-13} s, or $E_a < 0.58$ eV for $\tau_0 = 10^{-12}$ s, respectively. Already Darby and Wayman have argued that the gold-graphite binding energy, due to mainly van der Waals interaction, should be very small compared with the gold-gold binding energy (cohesive energy 3.8 eV).[3]

Given an upper limit of E_a, a rough estimate of the diffusion barrier E_d on graphite can be inferred from the initial nucleation density, and from the distance between particles, at which competitive capture becomes pronounced. Apparently, this amounts to the order of a few 100 nm, at room temperature. Given the adatom diffusion coefficient $D = (a^2/4\tau_0)\exp(-E_d/kT)$, with a as hop distance, the mean diffusion length λ depends on the difference of the energies for adsorption and diffusion, and on temperature:

$$\lambda = \frac{\alpha}{2} \exp\left\{\frac{E_a - E_d}{2kT}\right\}. \tag{1}$$

Thus, in our case, E_d is expected be smaller than about 0.3 eV.

A major goal of our present work is to obtain a more accurate estimate by simulating the dependence of the capture rate on the size of the capture area on the basis of a simple model of adatom diffusion, capture, and particle growth. This, however, requires us to correlate the evolution of the particle size and shape during growth with adatom kinetics and capture by direct impingement, both on the substrate and on the particle surface. Such correlations have been investigated in detail by Bermond and Venables.[15] Competition between adatom flux by direct impingement and by diffusion over the substrate, besides the tendency to assume the equilibrium shape by diffusion over the particle surface, is deemed responsible for kinetically determined crystallite shapes far from equilibrium. Especially, the existence of thin flat crystallites is attributed to a lack of kink sites for adatom incorporation and unfavored 2D nucleation on the particle surface. In our case of dendritic Au particles, we have to take into account in addition a potential barrier against diffusion across the particle edges, as is suggested by our observations of only very slowly filled channels and holes near the center of the particles. Estimates for the diffusion barrier on flat metal surfaces and for additional barriers at step edges have been obtained recently from STM work, as well as from theoretical calculations.[16–21]

Günther *et al.* have investigated by STM the nucleation and growth of monolayer islands of Au on reconstructed Au(100) faces.[16] On the basis of a rate equation analysis of island densities, they conclude that the adatom diffusion barrier should be about 0.2 eV. A value of this order may also hold for the (111) face, as its structure is rather similar to that of the ''hex''-reconstructed atoms in the top layer of the (100) surface. Boisvert *et al.* performed first-principle calculations for several metals and report a value for E_d of 0.22 eV for a Au monomer on Au(111).[17] For the same case, Stoltze calculated values between 0.10 and 0.13 eV using effective-medium theory.[18] Thus, the diffusion barrier of a Au atom on Au(111) appears to be of similar order as on HOPG, or possibly even lower. However, adatom transport between the surfaces of the graphite substrate and the dendrite mesas may be hindered by an additional Ehrlich-Schwoebel barrier. While Kyuno and Ehrlich[20] recently addressed the formation of various types of such barriers in general, experimental data for Au on Au(111) are lacking, to our knowledge. Meyer *et al.* applied a quantitative model to STM results for Ag on Ag(111) and Pt on Pt(111), and calculated the heights of this additional barrier to 0.15 and 0.165 eV, respectively.[21] Values of this order agree well with the calculated diffusion barrier of 0.26 eV for a Au atom descending over a monolayer step on Au(111) by Stoltze.[18] In fact, an additional barrier of 0.1 eV would reduce the diffusion coefficient by a factor of about 50. Therefore, and because of our observations of unfilled holes and channels in the dendritic particles, we assume in the following in a first approximation that such a barrier virtually prevents diffusion of Au atoms down the edges of the particles.

Indications are that adatom transfer from the side face of a particle to the top face is also not significant. One argument comes from calculations and measurements of the increase of the mean height of the particles during growth. The integrated contribution of direct impingement R_{imp} can be calculated from the deposition rate R_d and the (experimentally measured) increase with time of the projected area $F(t)$:

$$R_{\mathrm{imp}} = R_d \int_0^t F(t)\,dt. \tag{2}$$

Multiplication with the atomic volume v yields the integrated volume incorporated into the particle up to time t. The

increment in height, Δh, can be approximated by distributing this volume over the actual projected area of the particle at time t:

$$\Delta h(t) = \frac{R_{\mathrm{imp}} v}{F(t)} \tag{3}$$

and the total height is $h(t) = h_0 + \Delta h(t)$. Calculations for individual particles resulted in values of Δh between 1 and 1.5 nm at the end of deposition. This corresponds well with EDX analyses mentioned above, which have revealed that the mean particle height is of the order of 1 nm at the early stages, and increases to about 2 nm at the end of deposition. Therefore, the thickening of the particles may be attributed to direct impingement alone. This means that we can separate vertical from lateral growth. However, we will show in the following that the lateral growth speed is significantly influenced by the increase in height.

A growing particle represents a sink for adatom diffusion. This is usually expressed by a reduced local adatom concentration $n(r)$, with r being the distance from the edge of a particle:

$$n(r) = N\left\{1 - \frac{K_0\left(\frac{r}{\lambda}\right)}{K_0\left(\frac{R}{\lambda}\right)}\right\}, \tag{4}$$

where K_0 is a Bessel function of zero order, R is the radius of the (assumed spherical) particle, and N is the adatom concentration at great distance. The second term in the curly brackets, the ratio of the Bessel functions, represents the capture probability $\phi(r)$ for adatoms by the particle. The total capture probability by the particle is calculated by integrating over the (assumed) circular capture area around the edge of the particle (R) up to the border of the capture zone (r_l). Multiplying this with the deposition rate R_d results in the total capture rate

$$\Phi(R) = 2\pi R_d \int_R^{r_l} \phi(r)\, dr. \tag{5}$$

This converts into the rate of captured volume $\Phi_v(r)$ by multiplying with the specific volume v of the gold atom, which is taken as $v = 0.014\ \mathrm{nm}^3$, corresponding to an atomic radius of 0.15 nm. The lateral growth rate of the dendritic particles can now be modeled on the basis of the growth in height as discussed above. For this, we transform $h(t)$ into $h(R)$, using the experimentally determined function $R(t)$. By dividing $\Phi_v(R)$ by $h(R)$, we get the lateral growth rate $W(R)$ as a function of R, expressed in nm^2/s:

$$W(R) = \frac{\Phi_v(R)}{h(R)}. \tag{6}$$

This takes into account that the lateral growth speed decreases further with increasing height. In fact, this is seen for most particles by the somewhat faster decrease of the growth rate than of the capture zone. Representative results of such calculations according to Eq. (6) are compared with experimental data for three particles in Fig. 8. For this, h_0 was assumed to 1 nm, as was discussed above. The calculated

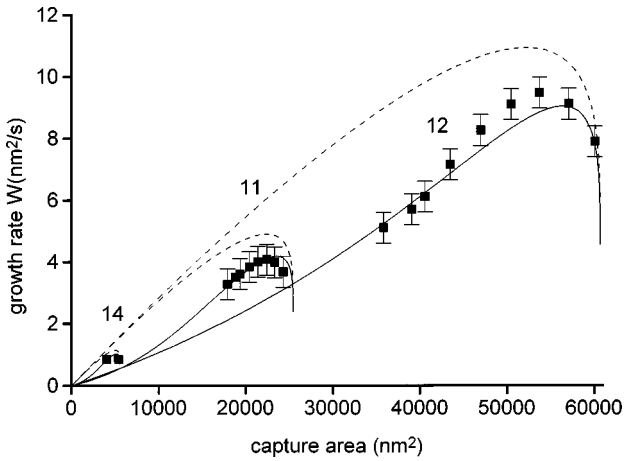

FIG. 8. Plot of measured and simulated lateral growth rates W of particles no. 11, 12, and 14 vs the individual sizes of the capture areas. The experimental data are obtained from differentiation of the curves in Fig. 7. Solid curves are calculated under the assumption that vertical growth starts with a height of 1 nm, and increases by additional 0.5 nm by direct impingement. Broken curves illustrate the case of constant height of 1 nm throughout growth. A best fit of the data was obtained with $E_a - E_d = 0.4$ eV (see text).

curves clearly show the increase of the growth speed at the early stages, which is due to the increasing capture probability with particle size. After passing a maximum, the subsequent decrease roughly corresponds to that of the respective capture area. These curves were calculated by taking into account vertical growth using Eqs. (2) and (3). In contrast, the broken curves were calculated for the (not realistic) case of constant thickness of the particles of 1 nm. Obviously, this would not reproduce the generally observed faster decrease of the growth speed than of the capture area. The experimental data were fitted by varying two parameters, namely the initial height and the energy parameter $\Delta E = E_a - E_d$. Assuming 1 nm for the initial height, a best simultaneous fit for all particles was obtained with $\Delta E = 0.4$ eV, corresponding to a mean adatom diffusion distance before desorption of about 400 nm. Increasing ΔE by 0.1 eV would result in much higher growth rates than observed, and would require reducing the initial height of the particle to 0.5 nm, corresponding to only about 2 ML of gold. This would appear rather unreasonable, taking into account the EDX results and the decent contrast of the aggregates. Therefore, we estimate the error margin for ΔE of the order of 0.05 eV. Taking $E_a = 0.64$ eV as an upper limit, according to Arthur and Cho,[8] the activation barrier for surface diffusion, E_d, would be no larger than 0.24 eV, and possibly even lower. It should be noted that the above calculations do not take into account the specific, dendritic shapes of the particles. Rather, mean radius values for assumed spherical particles were calculated from the projected areas of the aggregates. We believe that this approximation is justified, as a higher capture probability at the tips of the dendrites may be compensated by shadowing effects in the other inner parts of the aggregates.

V. CONCLUSIONS

Our *in situ* TEM analysis of the growth kinetics of quasi-two-dimensional gold particles on HOPG revealed interest-

ing details, which can be interpreted on the basis of a model of adatom diffusion and capture. As a main result, the growth speed of the dendritic gold aggregates can be directly correlated with the sizes of the respective capture areas, which are determined by competitive capture of adatoms by neighboring particles. Quantitative evaluation of the atomic capture rates became possible because evidence was found by EDX and image analysis that the heights of all the particles were rather similar, namely about 1 nm soon after nucleation, and increasing by direct impingement to about 1.5–2.0 nm at a substrate coverage of 40%, well in accordance with estimates by other authors.[2,5,10]

Further, EDX measurements revealed initially rather incomplete condensation on undisturbed substrate areas, with nucleation densities of below $10^9/\mathrm{cm}^2$ and dendritic growth of particles. This corresponds to results from the literature, where an initial condensation coefficient of below 5% is reported.[8] In contrast, condensation was found to be complete on disturbed areas, with number densities of finely dispersed particles of the order of $10^{11}/\mathrm{cm}^2$. This appears reasonable, as the distances between particles are much smaller than the mean adatom diffusion path length. Thus, the chances to escape capturing are extremely small.

Despite the relatively fast increase of substrate coverage with deposition time, the contribution of direct impingement from the vapor beam to lateral growth was found not to be significant. Rather, the faster decrease of the lateral growth speed than of the capture area can be explained by (relatively slow) vertical growth, which seems to be determined by direct impingement alone. Vertical growth of the side faces with many kink sites allows more atoms to attach, such that the lateral growth speed appears to decrease.

Evidence was found for the existence of an energetic barrier at the particle edges, similar to an Ehrlich-Schwoebel barrier at step edges of monatomic height, such that jumping of adatoms up and on to the top face, or vice versa down to the substrate, is not significant. Therefore, quantitative evaluation of the adatom diffusivity on the graphite substrate was possible by measuring the lateral growth rate of particles as a function of the capture area, and by fitting the data with calculations based on an adatom diffusion model, taking into account initially incomplete condensation, as well as the influence of vertical growth from direct impingement. As a result, a best fit of all data was obtained with a difference $\Delta E = E_a - E_d$ of the atomic energies of adsorption and diffusion of 0.4 (± 0.05) eV. Relying on the reported upper limit of the adatom lifetime of 10 ms at room temperature,[8] the diffusion barrier on graphite would be smaller than 0.24 eV.

It is interesting to compare these results with the case of amorphous carbon substrates, where condensation is complete at temperatures up to about 400 °C.[11] A similar value of about 0.4 eV has been found for ΔE, but with E_d of the order of 1.0 to 1.2 eV, being valid at least for higher temperatures.[9,12] It appears reasonable that ΔE reflects more a property of the carbon atoms but less of their crystallographic arrangement.

The type and the height of the Ehrlich-Schwoebel barrier could not be determined from our analysis. However, it may depend on the size and height of the particle. Also, the driving force for the particles to assume a thickness of the order of 1 nm soon after nucleation is not definitely known. One explanation may be the large cohesive energy of Au. Due to the weaker binding of Au to graphite, the step-edge barrier may be more easily overcome by adatoms at the edges of the particles when their thickness is lower. Recent deposition experiments at elevated temperatures also indicate such an influence on the growth kinetics, where the growth of well-faceted, flat particles with similar heights is observed. Details will be reported in a forthcoming paper.

ACKNOWLEDGMENTS

Thanks are due to Dr. J. A. Venables for fruitful discussions and for bringing further references to our attention.

[1] T. P. Darby and C. M. Wayman, J. Cryst. Growth **28**, 41 (1975); C. M. Wayman and T. P. Darby, *ibid.* **28**, 53 (1975).
[2] J. J. Métois, J. C. Heyraud, and Y. Takeda, Thin Solid Films **51**, 105 (1978).
[3] T. P. Darby and C. M. Wayman, J. Cryst. Growth **29**, 98 (1975).
[4] T. A. Witten and L. M. Sander, Phys. Rev. Lett. **47**, 1400 (1981).
[5] P. Wynblatt, J. J. Métois, and J. C. Heyraud, J. Cryst. Growth **102**, 618 (1990).
[6] R. Anton and M. Harsdorff, Vakuum-Technik **34**, 39 (1985); R. Anton, O. Reetz, and A. A. Schmidt, Ultramicroscopy **41**, 303 (1992).
[7] H. Melle and E. Menzel, Z. Naturforsch. A **33**, 282 (1978).
[8] J. R. Arthur and A. Y. Cho, Surf. Sci. **36**, 641 (1973).
[9] A. A. Schmidt, H. Eggers, K. Herwig, and R. Anton, Surf. Sci. **349**, 301 (1996).
[10] R. Nishitani, A. Kasuya, S. Kubota, and Y. Nishina, J. Vac. Sci. Technol. B **9**, 806 (1991).
[11] R. Anton, Vakuum-Technik **23**, 172 (1974).
[12] M. Paunov and M. Harsdorff, Z. Naturforsch. A **29a**, 1311 (1974).
[13] J. A. Venables, G. D. T. Spiller, and M. Hanbücken, Rep. Prog. Phys. **47**, 399 (1984).
[14] J. A. Venables, Surf. Sci. **299/300**, 798 (1994).
[15] J. M. Bermond and J. A. Venables, J. Cryst. Growth **64**, 239 (1983).
[16] S. Günther, E. Kopatzki, M. C. Bartelt, J. W. Evans, and R. J. Behm, Phys. Rev. Lett. **73**, 553 (1994).
[17] G. Boisvert, L. J. Lewis, M. J. Puska, and R. M. Nieminen, Phys. Rev. B **52**, 9078 (1995).
[18] P. Stoltze, J. Phys.: Condens. Matter **6**, 9495 (1994).
[19] K. Morgenstern, G. Rosenfeld, E. Laegsgaard, F. Besenbacher, and G. Comsa, Phys. Rev. Lett. **80**, 556 (1998).
[20] K. Kyuno and G. Ehrlich, Surf. Sci. **394**, L179 (1997).
[21] J. A. Meyer, J. Vrijmoeth, H. A. van der Vegt, E. Vlieg, and R. J. Behm, Phys. Rev. B **51**, 14 790 (1995).